ACS NANOSCIENCE Au
AN OPEN ACCESS JOURNAL OF THE AMERICAN CHEMICAL SOCIETY

pubs.acs.org/nanoau

Article

Effects of Immune Cell Heterogeneity and Protein Corona on the Cellular Association and Cytotoxicity of Gold Nanoparticles: A Single-Cell-Based, High-Dimensional Mass Cytometry Study

Sehee Park, My Kieu Ha, Yangsoon Lee, Jaewoo Song, and Tae Hyun Yoon*

Cite This: https://doi.org/10.1021/acsnanoscienceau.3c00001

Read Online

ACCESS | Metrics & More | Article Recommendations | Supporting Information

ABSTRACT: Understanding how nanoparticles (NPs) interact with biological systems is important in many biomedical research areas. However, the heterogeneous nature of biological systems, including the existence of numerous cell types and multitudes of key environmental factors, makes these interactions extremely challenging to investigate precisely. Here, using a single-cell-based, high-dimensional mass cytometry approach, we demonstrated that the presence of protein corona has significant influences on the cellular associations and cytotoxicity of gold NPs for human immune cells, and those effects vary significantly with the types of immune cells and their subsets. The altered surface functionality of protein corona reduced the cytotoxicity and cellular association of gold NPs in most cell types (e.g., monocytes, dendritic cells, B cells, natural killer (NK) cells, and T cells) and those immune cells selected different endocytosis pathways such as receptor-mediated endocytosis, phagocytosis, and micropinocytosis. However, even slight alterations in the major cell type (phagocytic cells and non-phagocytic cells) and T cell subsets (e.g., memory and naive T cells) resulted in significant protein corona-dependent variations in their cellular dose of gold NPs. Especially, naive T killer cells exhibited additional heterogeneity than memory T killer cells, with clusters exhibiting distinct cellular association patterns in single-cell contour plots. This multi-parametric analysis of mass cytometry data established a conceptual framework for a more holistic understanding of how the human immune system responds to external stimuli, paving the way for the application of precisely engineered NPs as promising tools of nanomedicine under various clinical settings, including targeted drug delivery and vaccine development.

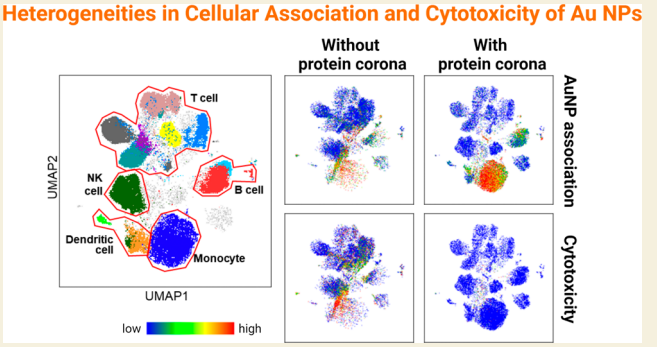

KEYWORDS: *mass cytometry, targeted drug delivery, gold nanoparticles, immune system, endocytosis, cytotoxicity*

INTRODUCTION

Understanding the interactions between nanoparticles (NPs) and biological systems is becoming increasingly relevant in many biomedical research areas such as targeted drug delivery,[1] vaccine development,[2−4] etc. However, it is well acknowledged that these interactions are exceedingly complicated to investigate, mostly caused by the heterogeneous nature of biological systems, such as the existence of numerous cell types with varying characteristics and multitudes of key environmental factors.[5] For targeted drug delivery, for example, a drug-loaded NP injected into a blood vessel will circulate through the body until it reaches the target organs or cells. However, as they travel through the bloodstream, they come into contact and interact with the immune system, which consists of diverse immune cells with varying phenotypes.[6−8] The interactions between the NPs and these immune cells begin with endocytosis, followed by intracellular trafficking and exocytosis, which are thought to be highly dependent on the types of immune cells as well as the physicochemical properties of the NPs and may result in significant variations in cytotoxicity.[6,7,9]

However, this is an ideal scenario for targeted drug delivery, and many other environmental factors exist in real-world clinical situations. Proteins in biological fluids, for example, can adsorb on the surface of NPs, forming a "protein corona", and influence the NP's subsequent interactions with biological cells.[9−11] For instance, during the preparation of nano-drugs, fetal bovine serum (FBS) (or bovine serum albumin [BSA]) has been often used to stabilize dispersions of NPs,[12,13] and these FBS-derived protein coronas are thought to modulate the surface functionality and agglomeration behaviors of NPs and

Received: January 12, 2023
Revised: April 12, 2023
Accepted: April 12, 2023

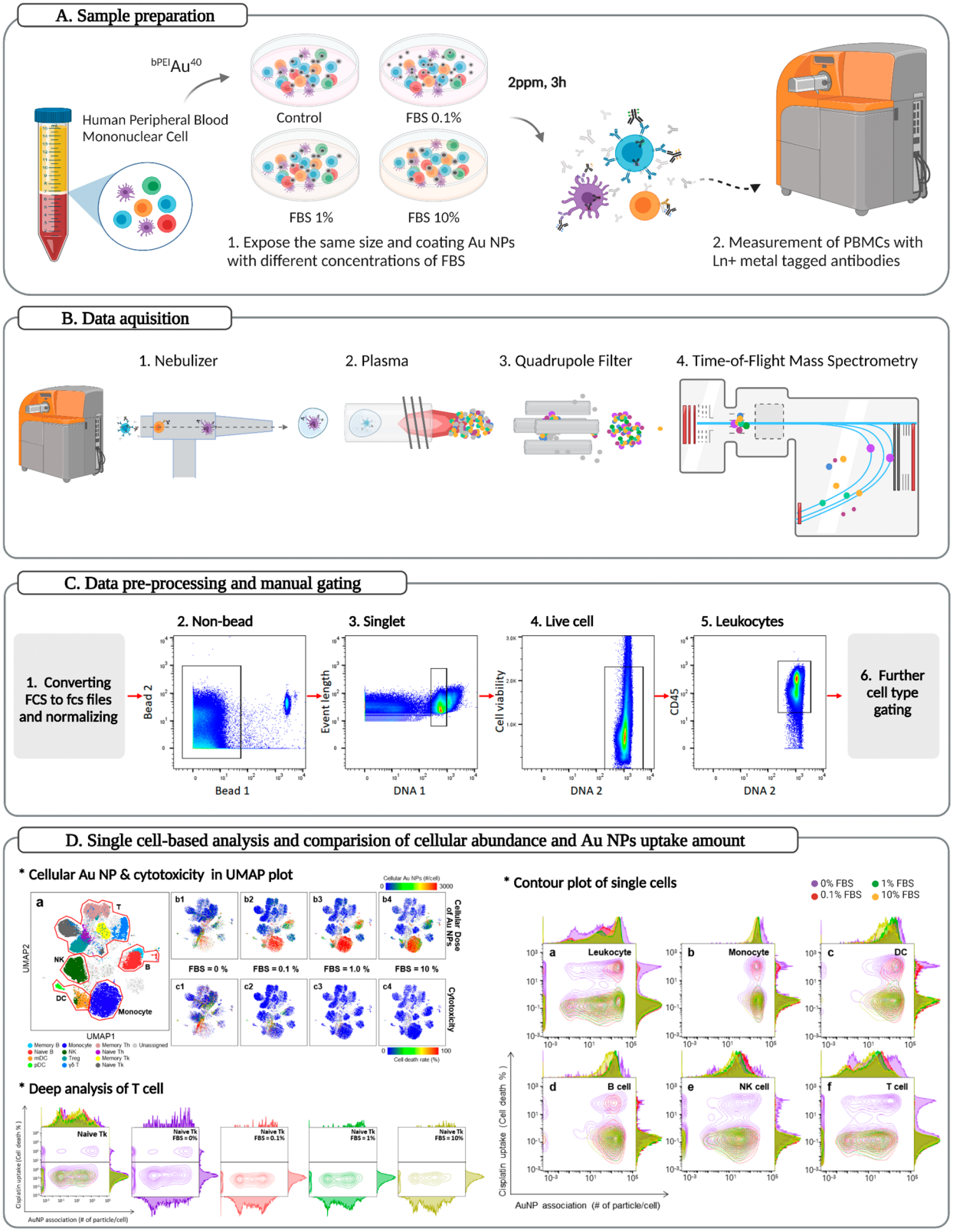

Figure 1. Workflow of mass cytometry experiment. (A) PBMCs were isolated from whole human blood by the density gradient method and treated with 2 μg/mL $^{bPEI}Au^{40}$ in RPMI media containing 0, 0.1, 1, and 10% FBS for 3 h. Au NP-treated cells were harvested and stained with 17 surface markers. (B) Metal-conjugated antibodies-tagged cells were introduced to mass cytometry, and FCS data were produced. (C) Normalize the FCS file and gate cell type manually by surface marker intensity. (D) Analyze the data using UMAP and contour plots of cell viability versus Au NP association.

affect the cellular association process and cytotoxicity of NPs.[10] Previous studies on these FBS-derived protein coronas have identified albumin, opsonin [e.g., immunoglobulin G (IgG) and antibodies], complement proteins, and apolipoproteins as

https://doi.org/10.1021/acsnanoscienceau.3c00001
ACS Nanosci. Au XXXX, XXX, XXX−XXX

the major components of the protein corona,[14−22] and a subsequent mass spectrometry (MS) study confirmed albumin as the most dominant protein adsorbed on the surface of Au NPs in cell culture media containing FBS.[23] While these changes in the surface functionality of NPs can influence the type of endocytosis pathways, proteins adsorbed on the surface of NPs can also alter the surface charge of the NPs, influencing their aggregation. The variations of the hydrodynamic sizes, caused by different degrees of agglomeration, may also lead to activation of different endocytosis pathways.[24] Earlier studies stated that the development of protein coronas prevents NP agglomeration and keeps their hydrodynamic sizes smaller. Larger NPs (>200 nm) are known to be more efficiently taken up by phagocytosis or macropinocytosis, but smaller NPs (100 nm) are favored by receptor-mediated endocytosis (RME) pathways such as clathrin-mediated endocytosis.[6] As a result, in the absence of a protein corona, phagocytosis and macropinocytosis may play essential roles in the cellular association of highly agglomerated NPs, while other RMEs may play major roles in the cellular uptake of less agglomerated, smaller NPs.

Due to their highly heterogeneous and interconnected nature, it would be better to study the human immune system and its interactions with NPs in a holistic manner, rather than conducting individual studies on each immune cell type. Peripheral blood mononuclear cells (PBMCs), a diverse mixture of highly specialized immune cells [e.g., monocytes, dendritic cells (DCs), natural killer (NK) cells, B cells, and T cells], are known to play key roles in human immune responses to external stimuli and are novel models for heterogeneous cellular systems. They are regarded as an important tool for researchers and clinicians working on human health and disease, since they can be used to examine the body's immune responses to numerous external stimuli, allowing us to better understand various diseases, design novel therapeutic treatments, and assess the efficiency of newly discovered drugs. PBMCs are good models to demonstrate the capability of mass cytometry, which have been employed as a substitute immune function model in the medical study area and toxicology applications.[25,26] Based on the study on PBMCs, we believe that this novel analytical approach can be expanded to include neutrophils and other polymorphonuclear cells such as eosinophils and basophils.

Conventional assays for assessing the toxicity or efficacy of NP-based drugs typically compare the administered dose of NPs to their cellular responses averaged over a large number of cells. Although these techniques are cheap, simple, rapid, and widely used, they may not adequately reflect the heterogeneous and interconnected nature of the human immune system interacting with NPs.[27] Therefore, to assess the toxicity or efficacy of NPs and understand their mechanisms in a holistic manner, there is a need to adapt novel analytical techniques and explore these biological processes multi-parametrically at a single-cell level. Mass cytometry, also known as cytometry by time-of-flight (CyTOF), is a recently established technology that analyzes cells multi-parametrically in a single-cell mode using metal-tagged cellular markers with minimal overlap of signals.[28] Mass cytometry allows for up to 50 metal isotope labels, which overcomes the limitations of fluorescence-based flow cytometry in terms of phenotyping and profiling immune cells by simultaneously detecting heterogeneous immune cell populations. This technique has gained prominence in biological and medical research over the last decade. Its capability of single-cell-based, high-dimensional data generation has facilitated deep profiling of highly heterogeneous immune cells,[29] monitoring disease progression or recovery,[30] and high-resolution profiling of cytokine expression and signaling responses.[31,32] Although it was introduced more than ten years ago and is now regarded as an established method of biomedical research, its competence in the areas of nanotoxicology and nanomedicine has not yet been fully exploited.[32−36]

In this study, to evaluate the general effects of cellular heterogeneity and FBS-derived protein corona on the cellular association and cytotoxicity of gold NPs (Au NPs) on human immune cells, we performed mass cytometry measurements on human PBMCs exposed to 6.2×10^9 (2 μg/mL) Au NPs in a cell culture medium with varying FBS concentrations of 0, 0.1, 1, and 10% (Figure 1). Major immune cell types (e.g., monocytes, dendritic cells, B cells, NK cells, and T cells) and their subsets [e.g., naive T killer cell (Tk)/T helper cell (Th), memory Tk/Th, regulatory T cell (Treg), and $\gamma\delta$ T cells] were assigned based on the surface marker expression of individual cells via a manual gating strategy (Figure S1), while cellular Au and Pt signals were measured to estimate the amount of cell-associated Au NPs and cellular death. The cellular dose and cytotoxicity of Au NPs were then presented as histograms and 2D contour plots to examine the effect of protein coronas and immune cell types on the cellular association and cytotoxicity of Au NPs, which provided valuable insights into the heterogeneous nature of the interactions such as the effect of FBS-derived protein corona on the cellular associations and cytotoxicity of Au NPs and their dependence on the types of immune cells and their subsets.

RESULTS AND DISCUSSION

Physicochemical Properties of Au NPs with FBS-Derived Protein Corona

We employed 40 nm branched polyethylenimine (bPEI)-coated Au NPs for assessing the effects of cellular heterogeneity and protein corona on the cellular association and cytotoxicity of Au NPs on human immune cells. The hydrodynamic size of bare Au NPs in deionized water (DW) was 50 nm, and this size increased in Roswell Park Memorial Institute (RPMI) media (Table S1). The hydrodynamic size increased with incubation time, and the protein corona generated with higher FBS concentrations (10%) had a smaller size than those generated with the lower FBS concentration (0%) (Figure S2). The bare NPs presented a zeta potential of 26 mV in DW, and the serum protein absorption on positively charged NPs led to a zeta potential decrement. On incubating with 1% FBS-supplemented RPMI, the NPs' zeta potential decreased significantly to −13 eV, suggesting the formation of a protein layer on NPs at low FBS concentrations (Table S1). However, the zeta potential did not change much until the FBS concentration reached 10%, showing that the protein corona's qualitative composition had not changed significantly. The protein contents in 10% FBS that coated the surface of NPs as 2.3×10^4 μg/cm^2, 1% FBS as 2.3×10^3 μg/cm^2, and 0.1% as 2.3×10^2 μg/cm^2. The bPEI-coated bare NPs' significantly positive zeta potential value may cause enhanced toxicity in cells due to its cationic nature,[37,38] and proteins in FBS may influence the degree of toxicity.

The absorbed proteins on FBS-derived protein corona were previously studied by sodium dodecyl sulfate−polyacrylamide gel electrophoresis (SDS−PAGE), liquid chromatography−

https://doi.org/10.1021/acsnanoscienceau.3c00001
ACS Nanosci. Au XXXX, XXX, XXX−XXX

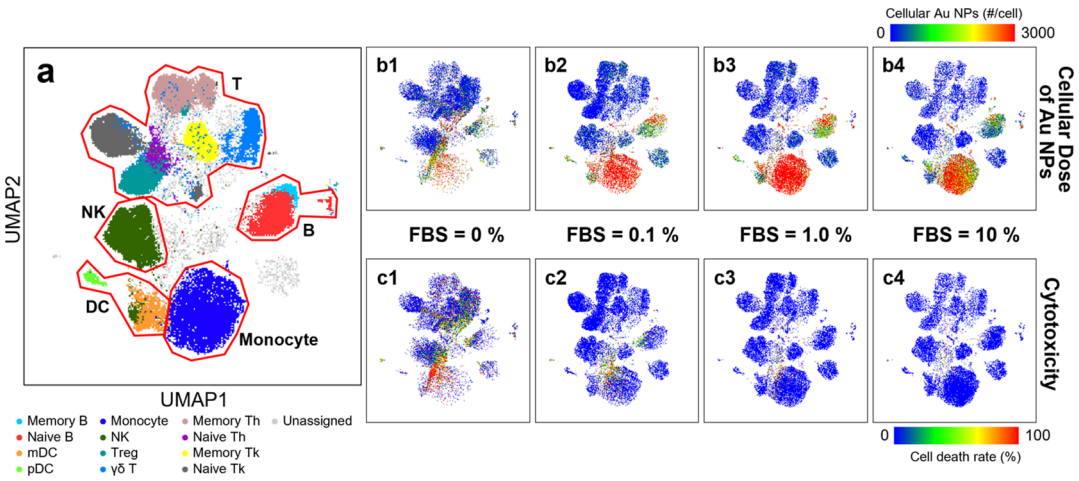

Figure 2. Immune cell profiling of human PBMCs cultured with different concentrations of FBS on UMAP visualization. (a) UMAP visualization of heterogeneous immune cells associated with protein corona gold NPs. Major cell types (e.g., monocytes, dendritic cells, B cells, NK cells, and T cells) are manually gated based on the expression of surface markers and are overlaid on UMAP plot. (b) Expression of cellular association with gold NPs at different concentrations of FBS and (c) their cytotoxicity for the human immune cells are represented on UMAP plot. The color profile indicates the degree of cellular Au NPs and cell death rate in FBS-dose-dependent manner. The expression of cytotoxicity was measured by cisplatin uptake of each cell types.

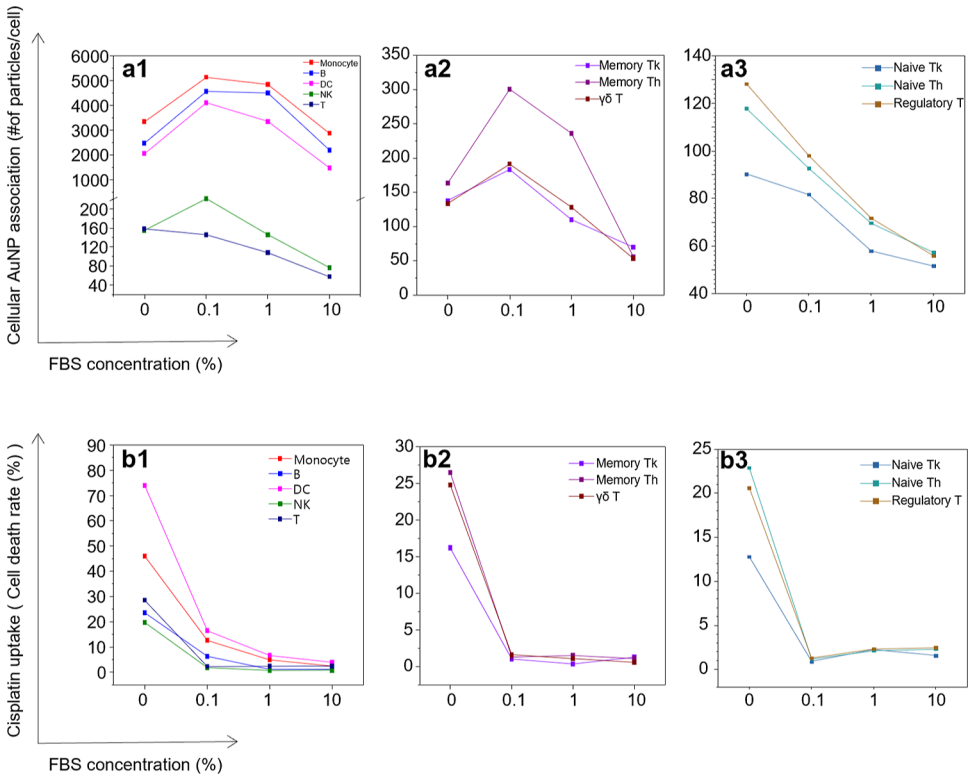

Figure 3. Au NP association and cell death rate comparison of major immune cell types. (a1−3) Cellular association of AuNPs of major immune cell types and T cell subsets at different concentrations of FBS. The total amount of cellular Au NP association in each cell type was averaged with total cell number. The major cell types (e.g., monocytes, dendritic cells, B cells, NK cells, and T cells) were compared (a1). T cells were further subdivided with CD4, CD8, CD45RA, and CD45RO (CD = cluster of differentiation) surface markers, and the cellular associations of T cells were calculated and compared (a2,a3), respectively. (b1−3) Cytotoxicity of major immune cell types and significant T cell subsets at different concentrations of FBS was analyzed. The cell death rate was calculated by cisplatin uptake and was normalized by the mean values of dead cells.

mass spectrometry/mass spectrometry (LC−MS/MS), and matrix-assisted laser desorption/ionization time-of-flight (MALDI-TOF) to identify the composition of proteins.[22,39,40] FBS-derived protein corona typically contains BSA, hemoglobin subunit alpha, apolipoprotein A-I, apolipoprotein E, α-2-HS-glycoprotein, and apolipoprotein A-II.[22,39,40] Particularly, proteins with lower molecular weight were enriched in the positively charged NPs.[21] In a study on the compositional evolution of adsorbed proteins of FBS-derived protein corona based on the amount of FBS, several protein bands with different protein masses were found even at low FBS

https://doi.org/10.1021/acsnanoscienceau.3c00001
ACS Nanosci. Au XXXX, XXX, XXX−XXX

concentrations, and the composition of hard corona remained stable across a wide range of FBS concentrations.[39]

Immune Cell Type-Dependent Variations of Cellular Au NPs and Their Cytotoxicity

Visualization and interpretation of high-dimensional mass cytometry is challenging. Therefore, it is necessary to adopt advanced data analysis algorithms for dimensionality reduction and visualization, such as t-distributed stochastic neighbor embedding (t-SNE) or uniform manifold approximation and projection (UMAP). Immune cell types, their populations, the cellular dose of Au NPs, and cytotoxicity were overlaid and compared on UMAP visualizations shown in Figure 2. Compared to the more widely used dimensionality reduction algorithm (i.e., t-SNE), UMAP is known to have the advantage of preserving intercluster (or global) information; cell types with similar characteristics are known to be located close to each other. As shown in Figure 2a, the manually gated immune cells overlaid on a UMAP visualization formed by four distinct regions: B cells on the right, monocytes and DCs on the bottom, NK cells on the left, T cells on the top. To explore variations in cellular doses and cytotoxicity of Au NPs in a qualitative manner, the cellular Au and Pt signals were also overlaid on the UMAP of the immune cells cultured and exposed to Au NPs under different FBS concentrations, as shown in Figure 2b1−b4,c1−c4. Overall, consistent with the previously reported LC50 values (75.44 μg/mL),[41] exposure to 2 μg/mL bPEI-coated Au NPs did not induce significant cytotoxicity in most of the immune cells, except for monocytes and DCs, which displayed much higher cellular association than others (Figure 2b1−b4,c1−c4). Similar to our previous studies on PBMCs exposed to Ag NPs,[42,43] the monocytes, DCs, and B cells seem to prefer association with Au NPs, while NK cells and some T cell subsets displayed less significant associations with the Au NPs. Additionally, as the FBS concentration changed, noticeable variations in the cellular Au NPs were observed. In contrast, the cytotoxicity of Au NPs seems to be strongly influenced by the presence/absence of protein corona, rather than immune cell types and the amount of cellular Au NPs.

Protein corona-dependent variations of the cellular Au NPs and their cytotoxicity at the level of cell types and their subsets.

To further investigate protein corona and immune cell type-dependent variations in cellular doses and cytotoxicity of Au NPs in a quantitative manner, the amounts of cellular Au NPs and cisplatin uptake were averaged for each major immune cell type and plotted for different levels of protein corona (Figure 3a1,b1). In general, increasing the concentration of FBS from 0.1 to 10% decreased the cellular association of the protein corona in all cell types. However, the FBS concentrations for the maximum cellular association of Au NPs varied with the type of immune cells. For instance, monocytes, DCs, and B cells displayed the maximum cellular Au NPs lying between the FBS concentrations of 0.1 and 1%, while NK cells displayed the maximum association of Au NPs at the FBS concentration of 0.1% (Figure 3a1). In contrast to other cell types, T cells had the highest association of cellular Au NPs at the FBS concentration of 0%, and the amounts of cell-associated Au NPs decreased with the increments of FBS concentration. Due to distinct characteristics of the T cells from the rest of the immune cells, we further investigated the subsets of T cells as shown in Figure 3a2−3,b2−3. In the case of some T cell subsets such as memory Th cells, memory Tk cells, and gamma delta T cells, the maximum levels of cellular Au NPs were observed at the FBS concentration of 0.1% (Figure 3a2). However, in cases of the other T cell subsets (i.e., naive Th cells, naive Tk cells, and regulatory T cells) with the lowest levels of cellular Au NPs, the maximum levels of cellular Au NPs were observed in the absence of protein corona, which continuously decreased with increasing FBS concentration (Figure 3a3). These observations clearly showed that the protein corona has immune cell-type or cellular subset-dependent influences on the cellular association of Au NPs and indicates that different cellular association mechanisms might be involved in different immune cell types and their subsets.

The immune cell-type-dependent associations of Au NPs under different coverages of the protein corona can be explained by the physicochemical properties (hydrodynamic size and surface functionality) of Au NPs as well as the nature of these immune cell types. Monocytes and DCs are professional phagocytic cells that are likely to associate with Au NPs via their unique phagocytic endocytosis processes, while the other immune cells internalize Au NPs through non-phagocytic endocytosis processes, such as macropinocytosis and RMEs. Phagocytosis is usually initiated by the adsorption of opsonins (e.g,. IgG) onto the NP surface, and the opsonized NPs are recognized by phagocyte cells (e.g., monocytes, DCs, and macrophages) via specific ligand−receptor interactions, which activate a signaling cascade to form phagosomes and subsequent internalization of NPs.[44−46] The RME pathways are also initiated by cargo molecules binding to cell surface receptors and allow only receptor-specific NPs to enter, whereas macropinocytosis does not involve specific protein receptors and mediates non-selective and non-specific NP uptake.[47] As mentioned earlier in the introduction, highly agglomerated, larger NPs (>200 nm) are known to experience more efficient uptake by phagocytosis or macropinocytosis, whereas smaller NPs with limited agglomeration (∼100 nm) are preferred by RME pathways, such as clathrin-mediated endocytosis. As shown in Figure S2 and Table S1, we observed rapid agglomeration of Au NPs (up to 442 nm, after 3 h of incubation time) in the absence of protein corona, which significantly slowed down with the increment of FBS concentration (126 nm, after 3 h of incubation at 10% FBS). Therefore, in terms of hydrodynamic size, phagocytosis is preferred by the highly agglomerated Au NPs in the absence or low coverage of the protein corona.

However, phagocytosis is also strongly influenced by the surface functionality of the Au NPs, since it is known to occur through specific ligand−receptor interactions. Thus, from the perspective of surface functionality, phagocytosis is preferred by Au NPs-coated protein corona. These counteracting effects of hydrodynamic size and surface functionality agree well with our observation of the maximum cellular Au NPs for phagocytic cells (e.g., monocyte), located between the FBS concentrations of 0.1 and 1% (Figure 3a1). On the other hand, for non-phagocytic cells (NK cell and T cells), the macropinocytosis pathway is preferred in the absence or low coverage of protein corona by the highly agglomerated large Au NPs via non-specific interactions, while the RME pathways are preferred by the smaller, less-agglomerated Au NPs coated with protein corona. Therefore, as the FBS concentration in the cell culture media increases, the contribution from the macropinocytosis pathway decreases, while the contribution from the RME pathways will increase. These counteracting

https://doi.org/10.1021/acsnanoscienceau.3c00001
ACS Nanosci. Au XXXX, XXX, XXX−XXX

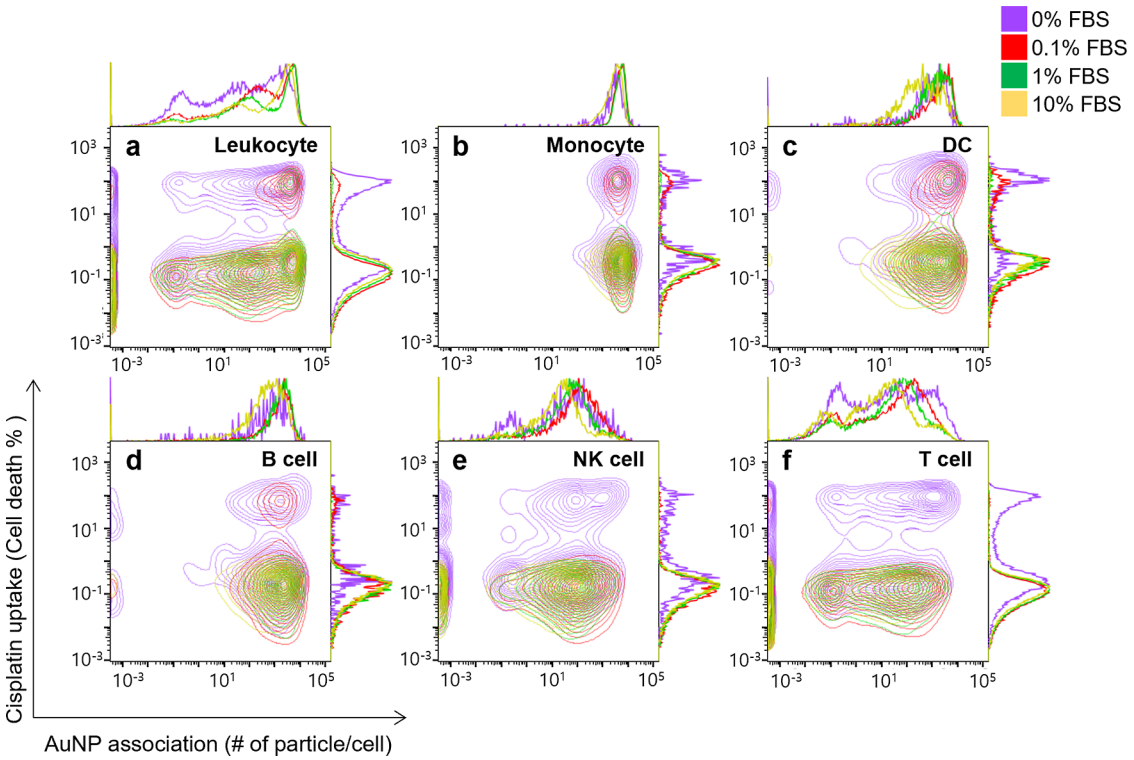

Figure 4. Cell-type-specific alteration of cell−Au NP association and cytotoxicity by protein corona at the single-cell level. Contour plots with histogram of cell death rate against cellular Au NP association (in number of particle) in the total leukocytes (a), monocytes (b), dendritic cells (c), B cells (d), NK cells (e), and T cells (f) exposed to AuNPs with different concentration of FBS. Au NP association in number of particles was calculated by ^{197}Au intensity, and cell death rate of each condition was normalized by the mean cisplatin uptake values of dead cells.

effects of micropinocytosis and RME pathways may explain our observations in Figure 3a1,a2. The NK cells (Figure 3a1) and some T cell subsets (memory Th/Tk cells and gamma delta T cells, shown in Figure 3a2) displayed maximum cellular association of Au NPs at the FBS concentration of 0.1%, which may indicate a major contribution from the macropinocytosis pathway for these immune cells, compared to the RME pathways. Moreover, as shown in Figure 3a3, the amount of cellular Au NPs for the naive Th/Tk and Treg cells is inversely proportional to the concentration of FBS in culture media, indicating predominant contributions from the macropinocytosis pathway in these immune cell types via non-specific associations of highly agglomerated Au NPs. As previously noted, the influence of protein corona on cytotoxicity was greater than that of the immune cell type, and the cytotoxicity was reduced as the FBS concentration increased (Figure 3b1). All types of immune cells demonstrated the greatest cytotoxicity in the absence of protein corona. While the protein corona and the type of immune cells and their subsets have a substantial effect on the cellular associations of Au NPs, the cytotoxicity of Au NPs appears to be controlled more by the presence/absence of protein corona, rather than by immune cell types. Additionally, these findings suggested that the protein corona may have influenced intracellular trafficking and exocytosis and caused dramatic reduction in the cytotoxicity of Au NPs coated with protein corona.[48−50]

Effects of Protein Corona and Cellular Heterogeneity on the Cellular Association and Cytotoxicity of Au NPs at the Single-Cell Level

To further investigate the heterogeneity of the cellular association and cytotoxicity of Au NPs at the single-cell level, we plotted them in contour plots and histograms for various immune cell types cultured under different concentrations of FBS. As shown in Figure 4a, total leukocytes displayed highly heterogeneous distributions in both cellular association and cytotoxicity profiles of the Au NPs. These histograms demonstrated that the leukocytes were widely distributed along both axes, as clusters with different levels of cellular association (low [less than a few particles per cell], medium [10^{-2} to 10^{3} particles per cell], and high [over 10^{3} particles per cell]) and cytotoxicity (e.g., low and high). In contrast with the diagonally elongated islands observed for the immune cells exposed to Ag NPs;[42,43] the horizontally elongated islands observed in this study indicate that there are no significant dose−response relationships in these clusters.

However, the populations of individual clusters were highly dependent on the presence or the absence of protein corona. The leukocytes exposed to the Au NPs without protein corona (purple) dominate the clusters with higher cytotoxicity, while those treated with Au NPs coated with protein corona (red, green, and yellow) mostly distribute in the clusters with lower cytotoxicity. Close observations of histograms and contour plots for each immune cell type revealed that the heterogeneous distributions in both the cellular association and cytotoxicity of Au NPs are highly dependent on the type of immune cells as well as the presence or the absence of a protein corona.

As shown in Figure 4b−d, monocytes, DCs, and B cells were mostly found as unimodal distributions in the medium to high levels of cellular Au NPs. On the contrary, as shown in Figure 4e,f, NK cells and T cells were widely distributed as bimodal or trimodal distributions from low to high levels of cellular Au NPs as well as significant cell populations with no Au signals.

https://doi.org/10.1021/acsnanoscienceau.3c00001
ACS Nanosci. Au XXXX, XXX, XXX−XXX

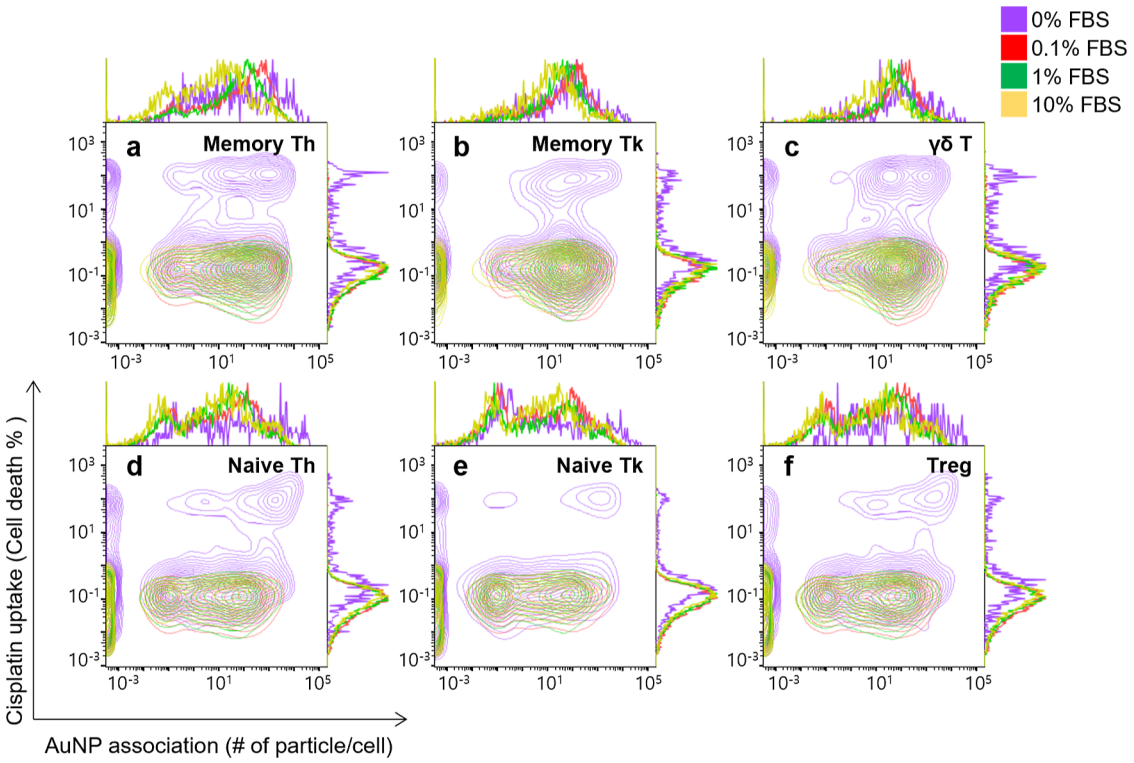

Figure 5. Contour plots and histograms for the T cell subsets on cellular association of Au NPs and their cytotoxicity. T cells are subdivided into (a) memory T helper cells, (b) memory T killer cells, (c) $\gamma-\delta$ T cells, (d) naive T helper cells, (e) naive T killer cells, and (f) regulatory T cells.

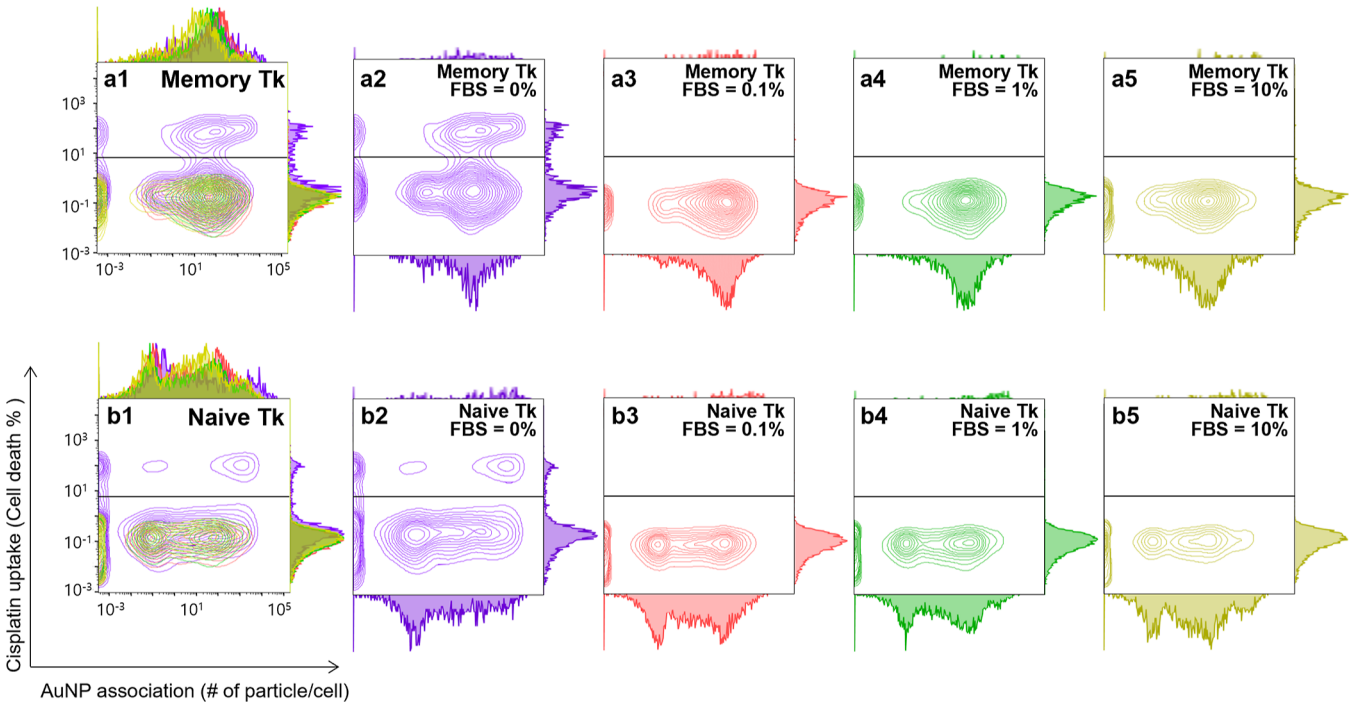

Figure 6. In-depth comparison of T killer cell populations according to cell viability. Contour plots and histograms for the memory (a) and naive (b) T killer cell subsets on cellular association of AuNPs and their cytotoxicity at different FBS concentrations. Based on the cell death rate of 5%, the clusters are divided into unhealthy (up) and healthy (down) cells. The integrated contour plots (a1,b1) are separated into individual contour plots according to the concentration of FBS. Different concentrations of FBS were used and compared significant effects of protein corona with Au NPs (a2–a5,b2–b5).

The contour plots of the monocytes, DCs, and B cells displayed two vertically separated oval-shaped islands, while those of NK cells and T cells were found to be two horizontally elongated islands. The absence of the diagonally elongated islands in these contour plots of various immune cell types confirmed that there were no significant dose–response

https://doi.org/10.1021/acsnanoscienceau.3c00001
ACS Nanosci. Au XXXX, XXX, XXX–XXX

relationships within these clusters. However, similar to the histogram of leukocytes, the cytotoxicity histograms for individual cell types displayed well-separated, bimodal distributions. More importantly, the higher cytotoxicity islands were significantly enhanced in the absence of protein corona (colored purple), which confirmed our earlier observations of dramatic cytotoxicity enhancements in the absence of protein corona (Figure 3b1−b3).

One of the most intriguing features of Figure 4 is that these contour plots are made up of multiple clusters, rather than a single unimodal distribution of cellular Au NPs and their cytotoxicity, which we typically assume during the interpretation of conventional dose−response relationships based on averaged values. These clusters with the distinct cellular association and cytotoxicity features imply that they may have evolved from distinct cellular subsets with different endocytosis and/or cytotoxicity mechanisms. In particular, the T cell contour plot shown in Figure 4f demonstrates the most heterogeneous feature, trimodal distributions of cellular Au NPs associated with bimodal cytotoxicity distributions. As shown in Figure 3a2,a3, the average number of Au NPs in these T cells and their subsets was typically less than 300. However, as illustrated by the contour plot in Figure 4f, there were clusters of T cells that were actually associated with over 1000 Au NPs and exhibited marked cytotoxicity, whereas a significant number of T cells were also found to be associated with no Au NPs. These findings in Figure 4f corroborate previous evidence of the importance of cellular subsets, as demonstrated in Figure 3a2,a3, where T cell subsets, such as memory Th/Tk cells and naive Th/Tk cells, exhibited distinct behaviors in their cellular association with Au NPs and may provide additional knowledge about the influence of cellular heterogeneity at the single-cell level. Thus, to further examine the effect of cellular heterogeneity on the cellular association of Au NPs with T cell subsets, the histograms and contour plots of various T cell subsets are given in Figure 5.

While the majority of T cells exhibiting high cytotoxicity can be attributed to those exposed to Au NPs in the absence of protein corona, as illustrated in Figure 5a−f, memory Tk/Th and gamma delta T cell clusters exhibit high cytotoxicity at low to medium levels of cellular Au NPs, whereas naive Tk/Th and Treg cell clusters exhibit high cytotoxicity only when associated with large numbers of Au NPs. When it comes to T cell clusters with low cytotoxicity, unimodal clusters widely distributed across a broad range of cellular Au NPs were observed predominantly in memory Tk/Th and $\gamma\delta$ T cells, whereas bimodal distributions with an additional cluster located at a low level of cellular Au NPs were observed exclusively in naive Tk/Th and Treg cells. We have highlighted the aforementioned differences more clearly in Figure 6, with the examples of memory and naïve Tk cells. In the high cytotoxicity region, memory Tk cells displayed an ellipsoidal, horizontally elongated cluster centered at medium levels of cellular Au NPs (Figure 6a1−a5). In contrast, the center of the oval-shaped naive Tk cell cluster moved to the right side with higher levels of cellular Au NPs (Figure 6b1−b5). Although both naive and memory Tk cells had horizontally elongated clusters in the low cytotoxicity zone, memory Tk cell distributions were found to be unimodal, centered at medium levels of cellular Au NPs. The naive Tk cells, on the other hand, had bimodal or trimodal distributions, with maximal populations located at low, medium−high, and/or high levels of cellular Au NPs. These observations at the single-cell level, particularly those of the naive Tk cells shown in Figure 6b1−b5, imply that there might be further subsets of naive Tk cells with distinct behaviors of cellular associations with Au NPs.

Our observations in this study demonstrate that even slight alterations in cellular subsets that arise during the cellular differentiation process can result in major disparities in their interactions with NPs. Naïve T cells, created in the thymus and released into the bloodstream, are recognized as essential components of the human immune system fighting with new and unrecognized infections and diseases. As a follow-up of the innate response's inflammatory environment, adaptive immune cells (activated T cells) proliferate and differentiate into cells with a range of functions suited for the immunological challenge. Upon eradication of the invading pathogen, the majority of adaptive cells die by apoptosis, while an array of memory cell subsets remains. These memory cells have a variety of migratory features and activities, which work together to mediate a quick and protective immune response in the event of reinfection.[51] It is well established that memory and naive T cells respond to antigens in a qualitatively different way. The activation threshold of memory T cells is lower than that of naive T cells, indicating that memory T cells are able to respond to antigens at lower concentrations than naive T cells. Between naïve and memory T cells, there are several phenotypic differences that occur mostly during the initial T cells activation process and appear to persist in memory cells. Particularly, differences in the expression of molecules involved in cell surface adhesion (e.g., beta 1 (CD29, CD49d, and CD49e) and beta 2 (CD11a, CD11b, and CD18) integrins, CD2, CD44, CD54, and CD58) and lymphocyte migration (CD62L and CC chemokine receptor 7), as well as other cell surface molecules, such as CD122, Ly-6C, and CD45, are noticeable.[52]

For example, as demonstrated in the manual gating strategy shown in Figure S1, naïve and memory subsets of both Tk and Th cells were identified by their expression of surface markers (CD45RA and CD45RO), denoted as CD45RA+/CD45RO− and CD45RA−/CD45RO+, respectively. CD45 is known to have eight isoforms with highly glycosylated extracellular domains that extend linearly from the cell membrane and allow for a great deal of diversity in the structure of their side chains. Among these eight CD45 isoforms, naïve T cells normally express CD45RA, which has just the A protein region, whereas memory T cells typically express CD45RO, the shortest CD45 isoform that contains none of the A, B, or C protein sections.[53] This slight difference in glycosylated extracellular domains of CD45 isoforms may account for the observed variations between the contour plots of memory and naive Tk cells shown in Figure 6. Even though mass cytometry cannot distinguish between intracellular and membrane-bound Au NPs, it has advantages over microscopic methods for analyzing heterogeneous cells like PBMCs in terms of high throughput and high dimensionality.

CONCLUSIONS

In this study, using a single-cell-based, high-dimensional mass cytometry approach, we demonstrated that the presence of FBS-derived protein corona has a significant effect on the cellular associations and cytotoxicity of Au NPs on human immune cells. In a cell culture medium with varied FBS concentrations of 0, 0.1, 1, and 10%, Au NPs exhibited the lowest cytotoxicity and cellular association in the 10% FBS condition. These effects are highly dependent on the types of

https://doi.org/10.1021/acsnanoscienceau.3c00001
ACS Nanosci. Au XXXX, XXX, XXX−XXX

immune cells and their subsets, particularly those memory and naive T cell subsets among monocytes, dendritic cells, B cells, NK cells, and T cells.

Nevertheless, given the heterogeneous and interconnected nature of NPs' interactions with various immune cell types as well as the numerous parameters involved in this process, it is necessary to conduct more comprehensive studies on the various parameters influencing the endocytosis pathways of NPs interacting with heterogenous immune cells, such as physicochemical properties and protein corona compositions of NPs on the endocytosis mechanisms. Furthermore, the influences of the NPs and protein corona on immune cell differentiation need to be studied for the applications in precision nanomedicine.

Although its capability has not been fully exploited in the area of nanomedicine yet, high-dimensional mass cytometry that analyzes cells multi-parametrically in a single-cell mode can overcome the current limitations of biological assays by simultaneously measuring the amounts of cell-associated NPs as well as phenotyping heterogeneous immune cell populations. For instance, additional mass cytometry research on the impacts of specific protein compositions of protein corona will help us understand the roles of individual proteins on the cell type-dependent association of NPs and resulting cytotoxicity. Additionally, since we have paved the way for the use of mass cytometry in these studies, a future study may potentially focus on protein corona made from human serum or other biomolecules. We believe that this novel analytical approach can be expanded to include neutrophils, other polymorphonuclear cells (such as eosinophils and basophils), and tissue cells.

The clinical studies on the safety or efficacy of nanomaterials can be conducted at a considerably later stage of nano drug development, only for a small number of nanomaterial candidates and after much more consideration and validation. However, we also believe that our study combining an in vitro system with human PBMCs and a novel mass cytometry approach will accelerate the application of NPs in a variety of clinical settings by providing a more comprehensive and systematic understanding of the influences of the key parameters.

MATERIALS AND METHODS

Materials

Branched polyethylenimine (bPEI)-coated 40 nm Au NPs, $^{bPEI}Au^{40}$ NPs, from NanoComposix (San Diego, CA, USA) were used in this study. The physicochemical characterization of $^{bPEI}Au^{40}$ NPs (i.e., hydrodynamic size and zeta potential) was performed using DLS (Zetasizer Nano ZS90; Malvern Panalytical), and the results are presented in Table S1 and Figure S2. The hydrodynamic size was measured at 25 °C under different dispersion conditions: 2 μg/mL (6.2×10^9 particles) in distilled water and RPMI-1640 medium (Lonza BioWhittaker, USA) containing 10, 1, 0.1, and 0% FBS (Gibco, USA). Before use, the NP suspensions were dispersed by 5 min sonication and 1 min vortex, and time-series measurements were taken every hour from 0 to 3 h. The core size was measured by TEM (JEM 2100F; JEOL), and the TEM images and size distributions are presented in Figure S3.

Isolation of PBMCs from Whole Blood

The human blood samples used in this study were obtained from Yonsei University Hospital (Seoul, Republic of Korea) with informed consent from the donors and approval from the Institutional Review Board (no. HYUH 2018-09-005-004). Human blood samples were collected from healthy donors into ethylenediaminetetraacetic acid hematology tubes to prevent blood coagulation, and PBMCs were isolated from whole blood using the density gradient method. Whole blood and Dulbecco's phosphate-buffered saline (DPBS, Welgene, Korea) were mixed in a 1:1 ratio, and diluted blood was placed on the Ficoll−Paque PLUS (GE Healthcare Bio-Sciences, Sweden) layer in centrifuge tubes. These tubes were centrifuged in a swing-bucket rotor centrifuge (model 1248R, Labogene, Korea) at 400g and 25 °C for 40 min. After centrifugation, the PBMC layer was collected and washed in water and DPBS to remove the remaining red blood cells. Washed cells were dispersed in RPMI-1640 media (LonzaTM BioWhittakerTM, USA) supplemented with FBS for NP treatment.

Exposure of hPBMCs to Au NPs

Cells were transferred to 35 × 10 mm Petri dishes (SPL Life Sciences, Korea), and the number of cells in the cell culture media was adjusted to $1-2 \times 10^6$ cells/mL. 2 μg/mL (6.2×10^9 particles) Au treated samples of four conditions were prepared to identify the effect of surrounding serum protein amount on cell-NP interactions. Cells were treated with 2 μg/mL $^{bPEI}Au^{40}$ in RPMI media containing 0, 0.1, 1, and 10% FBS and incubated for 3 h at 37 °C and 5% CO_2. After incubation, Au NP-exposed cells were transferred to empty centrifuge tubes and washed with DPBS to remove extra NPs that did not enter the cell.

Surface Marker Staining

After washing with DPBS, cells were stained with cisplatin (Fluidigm Corp., USA) to check cell viability and barcoded using a Pd barcode (Cell-ID 20-Plex Pd Barcoding Kit, Fluidigm Corp., USA) to reduce marker intensity variation between samples. The cells were labeled with 17 surface markers according to the Maxpar Phosphoprotein Staining with Fresh Fix Protocol (Fluidigm Corp., USA), and the cell surface labeling panel is presented in Table S2. All markers in the labeling panel were purchased from Fluidigm Corp. USA. After surface staining, cells were fixed in formaldehyde (Thermo Scientific, USA) and dispersed in Cell-ID Intercalator-Ir (Fluidigm Corp., USA) solution overnight to check the DNA content of the cells.

Sample Loading and Data Acquisition

Cells were rewashed before data acquisition and suspended at 1×10^6 cells/mL per sample in the cell acquisition solution (Fluidigm Corp., USA). For normalization, calibration beads were added at 1:10 v/v, and cells were filtered into strainer-capped tubes just before the measurement using a Helios mass cytometer (Fluidigm Corp., USA). The blank solution (5% HNO_3) and a $AuNO_3$ solution (1 ng mL^{-1} in 5% HNO_3) were measured by the instrument to calibrate the ^{197}Au counts and after measuring these solutions, $^{bPEI}Au^{40}$-treated samples were loaded. The cellular Au NP association was calculated using the average dual count of ^{197}Au in the collected data.

Data Analysis

FlowJo (version 10.8.0, LLC, USA) and Cytobank (version 9.0, Inc., USA) were used for data gating and visualization. Raw data were transformed into an inverse hyperbolic sine (arcsinh), and cell types were identified by manual gating based on the surface markers (Figure S1 and Table S2). Quantification of cellular Au NPs was performed according to the method proposed by Ivask et al.[34] The UMAP method was used to visualize high-dimensional mass cytometry data at single-cell resolution (Figure 1). Quantitative data were plotted using the OriginPro software program (version 2016 b9.3.2.303 Academic, Origin Lab Corporation, USA). For the contour plot, we used 21,455, 72,409, 67,415, and 67,755 cells for 2 μg/mL-Au NP-treated cells incubated with 0, 0.1, 1, and 10% FBS, respectively.

ASSOCIATED CONTENT

Supporting Information

The Supporting Information is available free of charge at https://pubs.acs.org/doi/10.1021/acsnanoscienceau.3c00001.

Gating strategy, surface marker panel list, and more detailed information of NP and protein corona characterization (PDF)

https://doi.org/10.1021/acsnanoscienceau.3c00001
ACS Nanosci. Au XXXX, XXX, XXX−XXX

AUTHOR INFORMATION

Corresponding Author

Tae Hyun Yoon − *Department of Chemistry, College of Natural Sciences, Hanyang University, Seoul 04763, Republic of Korea; Research Institute for Convergence of Basic Science and Institute of Next Generation Material Design, Hanyang University, Seoul 04763, Republic of Korea; Yoon Idea Lab. Co. Ltd, Seoul 04763, Republic of Korea;* orcid.org/0000-0002-2743-6360; Email: taeyoon@hanyang.ac.kr

Authors

Sehee Park − *Department of Chemistry, College of Natural Sciences, Hanyang University, Seoul 04763, Republic of Korea*

My Kieu Ha − *Department of Chemistry, College of Natural Sciences, Hanyang University, Seoul 04763, Republic of Korea;* Present Address: Vaccine & Infectious Disease Institute, University of Antwerp, Antwerp 2610, Belgium

Yangsoon Lee − *Department of Laboratory Medicine, College of Medicine, Hanyang University, Seoul 04763, Republic of Korea*

Jaewoo Song − *Department of Laboratory Medicine, College of Medicine, Yonsei University, Seoul 03722, Republic of Korea*

Complete contact information is available at: https://pubs.acs.org/10.1021/acsnanoscienceau.3c00001

Author Contributions

Conceptualization, T.H.Y. Resources, Y.L., and J.S. Validation, S.P. and M.K.H. Formal analysis, S.P. Investigation, S.P. and M.K.H. Writing—original draft preparation, S.P. and T.H.Y. Writing—review and editing, T.H.Y., M.K.H., Y.L., and J.S. Visualization, S.P. Supervision, T.H.Y. Funding acquisition, T.H.Y., Y.L., and J.S., All authors contributed to the article and approved the submitted version. CRediT: **Sehee Park** formal analysis (lead), investigation (lead), validation (lead), visualization (lead), writing-original draft (lead); **My Kieu Ha** investigation (supporting), validation (supporting), writing-review & editing (supporting); **Yangsoon Lee** funding acquisition (equal), resources (equal), writing-review & editing (supporting); **Jaewoo Song** funding acquisition (equal), resources (equal), writing-review & editing (supporting); **Tae Hyun Yoon** conceptualization (lead), funding acquisition (equal), supervision (lead), writing-original draft (supporting), writing-review & editing (lead).

Notes

The authors declare no competing financial interest.

ACKNOWLEDGMENTS

This research was supported by the Basic Science Research Program through the National Research Foundation of Korea (NRF) [grant number 2020R1A6A1A06046728] and Korea Basic Science Institute (National Research Facilities and Equipment Center) [grant number 2019R1A6C1030014], both funded by the Ministry of Education. This research was also partially supported by the Nano Material Technology Development Program [grant number 2021M3A7B6031397] of the National Research Foundation of Korea funded by the Ministry of Science and ICT.

ABBREVIATIONS

NP	nanoparticle
FBS	fetal bovine serum
BSA	bovine serum albumin
IgG	immunoglobulin G
PBMC	peripheral blood mononuclear cell
DC	dendritic cell
RME	receptor-mediated endocytosis
CyTOF	cytometry by time-of-flight
bPEI	branched polyethylenimine
DW	deionized water
RPMI	Roswell Park Memorial Institute
SDS-PAGE	sodium dodecyl sulfate-polyacrylamide gel electrophoresis
LC−MS/MS	liquid chromatography−tandem mass spectrometry
MALDI-TOF	matrix-assisted laser desorption/ionization time-of-flight
CD	cluster of differentiation
Th	T helper cell
Tk	T killer cell
Treg	regulatory T cell
t-SNE	t-distributed stochastic neighbor embedding
UMAP	uniform manifold approximation and projection
NK	natural killer cell
DLS	dynamic light scattering
TEM	transmission electron microscopy
DPBS	Dulbecco's phosphate-buffered saline

REFERENCES

(1) Mitchell, M. J.; Billingsley, M. M.; Haley, R. M.; Wechsler, M. E.; Peppas, N. A.; Langer, R. Engineering precision nanoparticles for drug delivery. *Nat. Rev. Drug Discovery* **2021**, *20*, 101−124.

(2) Lung, P.; Yang, J.; Li, Q. Nanoparticle formulated vaccines: opportunities and challenges. *Nanoscale* **2020**, *12*, 5746−5763.

(3) Chauhan, G.; Madou, M. J.; Kalra, S.; Chopra, V.; Ghosh, D.; Martinez-Chapa, S. O. Nanotechnology for COVID-19: Therapeutics and Vaccine Research. *ACS Nano* **2020**, *14*, 7760−7782.

(4) Li, J.; Chen, C.; Xia, T. Understanding Nanomaterial-Liver Interactions to Facilitate the Development of Safer Nanoapplications. *Adv. Mater.* **2022**, *34*, No. e2106456.

(5) Altschuler, S. J.; Wu, L. F. Cellular heterogeneity: do differences make a difference? *Cell* **2010**, *141*, 559−563.

(6) Behzadi, S.; Serpooshan, V.; Tao, W.; Hamaly, M. A.; Alkawareek, M. Y.; Dreaden, E. C.; Brown, D.; Alkilany, A. M.; Farokhzad, O. C.; Mahmoudi, M. Cellular uptake of nanoparticles: journey inside the cell. *Chem. Soc. Rev.* **2017**, *46*, 4218−4244.

(7) Rennick, J. J.; Johnston, A. P. R.; Parton, R. G. Key principles and methods for studying the endocytosis of biological and nanoparticle therapeutics. *Nat. Nanotechnol.* **2021**, *16*, 266−276.

(8) Blanco, E.; Shen, H.; Ferrari, M. Principles of nanoparticle design for overcoming biological barriers to drug delivery. *Nat. Biotechnol.* **2015**, *33*, 941−951.

(9) Dawson, K. A.; Yan, Y. Current understanding of biological identity at the nanoscale and future prospects. *Nat. Nanotechnol.* **2021**, *16*, 229−242.

(10) Corbo, C.; Molinaro, R.; Parodi, A.; Toledano Furman, N. E.; Salvatore, F.; Tasciotti, E. The impact of nanoparticle protein corona on cytotoxicity, immunotoxicity and target drug delivery. *Nanomedicine* **2016**, *11*, 81−100.

(11) Oh, J. Y.; Kim, H. S.; Palanikumar, L.; Go, E. M.; Jana, B.; Park, S. A.; Kim, H. Y.; Kim, K.; Seo, J. K.; Kwak, S. K.; Kim, C.; Kang, S.; Ryu, J. H. Cloaking nanoparticles with protein corona shield for targeted drug delivery. *Nat. Commun.* **2018**, *9*, 4548.

(12) ISO. Nanotechnologies—Compilation and description of sample preparation and dosing methods for engineered and manufactured nanomaterials. *ISO/TR 16196:2016(E) Nanotechnologies—Compilation and Description of Sample Preparation and Dosing Methods for Engineered and Manufactured Nanomaterials*, 2016.
(13) ISO. Biological evaluation of medical devices—Part 22: Guidance on nanomaterials. *ISO/TR 10993-22:2017(E) Biological Evaluation of Medical Devices—Part 22: Guidance on Nanomaterials*, 2017.
(14) Luck, M.; Pistel, K. F.; Li, Y. X.; Blunk, T.; Muller, R. H.; Kissel, T. Plasma protein adsorption on biodegradable microspheres consisting of poly(D,L-lactide-co-glycolide), poly(L-lactide) or ABA triblock copolymers containing poly(oxyethylene). Influence of production method and polymer composition. *J. Controlled Release* **1998**, *55*, 107−120.
(15) Gref, R.; Luck, M.; Quellec, P.; Marchand, M.; Dellacherie, E.; Harnisch, S.; Blunk, T.; Muller, R. H. 'Stealth' corona-core nanoparticles surface modified by polyethylene glycol (PEG): influences of the corona (PEG chain length and surface density) and of the core composition on phagocytic uptake and plasma protein adsorption. *Colloids Surf., B* **2000**, *18*, 301−313.
(16) Gessner, A.; Lieske, A.; Paulke, B. R.; Muller, R. H. Functional groups on polystyrene model nanoparticles: influence on protein adsorption. *J. Biomed. Mater. Res.* **2003**, *65A*, 319−326.
(17) Gessner, A.; Waicz, R.; Lieske, A.; Paulke, B.; Mader, K.; Muller, R. H. Nanoparticles with decreasing surface hydrophobicities: influence on plasma protein adsorption. *Int. J. Pharm.* **2000**, *196*, 245−249.
(18) Thode, K.; Luck, M.; Semmler, W.; Muller, R. H.; Kresse, M. Determination of plasma protein adsorption on magnetic iron oxides: sample preparation. *Pharm. Res.* **1997**, *14*, 905−910.
(19) Mortensen, N. P.; Hurst, G. B.; Wang, W.; Foster, C. M.; Nallathamby, P. D.; Retterer, S. T. Dynamic development of the protein corona on silica nanoparticles: composition and role in toxicity. *Nanoscale* **2013**, *5*, 6372−6380.
(20) Pozzi, D.; Caracciolo, G.; Digiacomo, L.; Colapicchioni, V.; Palchetti, S.; Capriotti, A. L.; Cavaliere, C.; Zenezini Chiozzi, R.; Puglisi, A.; Lagana, A. The biomolecular corona of nanoparticles in circulating biological media. *Nanoscale* **2015**, *7*, 13958−13966.
(21) Saha, K.; Rahimi, M.; Yazdani, M.; Kim, S. T.; Moyano, D. F.; Hou, S.; Das, R.; Mout, R.; Rezaee, F.; Mahmoudi, M.; Rotello, V. M. Regulation of Macrophage Recognition through the Interplay of Nanoparticle Surface Functionality and Protein Corona. *ACS Nano* **2016**, *10*, 4421−4430.
(22) Izak-Nau, E.; Voetz, M.; Eiden, S.; Duschl, A.; Puntes, V. F. Altered characteristics of silica nanoparticles in bovine and human serum: the importance of nanomaterial characterization prior to its toxicological evaluation. *Part. Fibre Toxicol.* **2013**, *10*, 56.
(23) Casals, E.; Pfaller, T.; Duschl, A.; Oostingh, G. J.; Puntes, V. Time evolution of the nanoparticle protein corona. *ACS Nano* **2010**, *4*, 3623−3632.
(24) Dai, Q.; Yan, Y.; Ang, C. S.; Kempe, K.; Kamphuis, M. M.; Dodds, S. J.; Caruso, F. Monoclonal antibody-functionalized multilayered particles: targeting cancer cells in the presence of protein coronas. *ACS Nano* **2015**, *9*, 2876−2885.
(25) Rahmoune, H.; Guest, P. C. Studies of Isolated Peripheral Blood Cells as a Model of Immune Dysfunction. *Methods Mol. Biol.* **2018**, *1735*, 221−229.
(26) Pourahmad, J.; Salimi, A. Isolated Human Peripheral Blood Mononuclear Cell (PBMC), a Cost Effective Tool for Predicting Immunosuppressive Effects of Drugs and Xenobiotics. *Iran. J. Pharm. Res.* **2015**, *14*, 979.
(27) Singh, S.; Carpenter, A. E.; Genovesio, A. Increasing the Content of High-Content Screening: An Overview. *J. Biomol. Screening* **2014**, *19*, 640−650.
(28) Bandura, D. R.; Baranov, V. I.; Ornatsky, O. I.; Antonov, A.; Kinach, R.; Lou, X.; Pavlov, S.; Vorobiev, S.; Dick, J. E.; Tanner, S. D. Mass cytometry: technique for real time single cell multitarget immunoassay based on inductively coupled plasma time-of-flight mass spectrometry. *Anal. Chem.* **2009**, *81*, 6813−6822.
(29) Newell, E. W.; Sigal, N.; Bendall, S. C.; Nolan, G. P.; Davis, M. M. Cytometry by time-of-flight shows combinatorial cytokine expression and virus-specific cell niches within a continuum of CD8+ T cell phenotypes. *Immunity* **2012**, *36*, 142−152.
(30) Amir, E. a. D.; Davis, K. L.; Tadmor, M. D.; Simonds, E. F.; Levine, J. H.; Bendall, S. C.; Shenfeld, D. K.; Krishnaswamy, S.; Nolan, G. P.; Pe'er, D. viSNE enables visualization of high dimensional single-cell data and reveals phenotypic heterogeneity of leukemia. *Nat. Biotechnol.* **2013**, *31*, 545−552.
(31) Behbehani, G. K.; Bendall, S. C.; Clutter, M. R.; Fantl, W. J.; Nolan, G. P. Single-cell mass cytometry adapted to measurements of the cell cycle. *Cytometry, Part A* **2012**, *81A*, 552−566.
(32) Yang, Y. S.; Atukorale, P. U.; Moynihan, K. D.; Bekdemir, A.; Rakhra, K.; Tang, L.; Stellacci, F.; Irvine, D. J. High-throughput quantitation of inorganic nanoparticle biodistribution at the single-cell level using mass cytometry. *Nat. Commun.* **2017**, *8*, 14069.
(33) Guo, Y.; Baumgart, S.; Stark, H. J.; Harms, H.; Muller, S. Mass Cytometry for Detection of Silver at the Bacterial Single Cell Level. *Front. Microbiol.* **2017**, *8*, 1326.
(34) Ivask, A.; Mitchell, A. J.; Hope, C. M.; Barry, S. C.; Lombi, E.; Voelcker, N. H. Single Cell Level Quantification of Nanoparticle-Cell Interactions Using Mass Cytometry. *Anal. Chem.* **2017**, *89*, 8228−8232.
(35) Orecchioni, M.; Bedognetti, D.; Newman, L.; Fuoco, C.; Spada, F.; Hendrickx, W.; Marincola, F. M.; Sgarrella, F.; Rodrigues, A. F.; Menard-Moyon, C.; Cesareni, G.; Kostarelos, K.; Bianco, A.; Delogu, L. G. Single-cell mass cytometry and transcriptome profiling reveal the impact of graphene on human immune cells. *Nat. Commun.* **2017**, *8*, 1109.
(36) Vanhecke, D.; Rodriguez-Lorenzo, L.; D Clift, M. J.; Blank, F.; Petri-Fink, A.; Rothen-Rutishauser, B. Quantification of nanoparticles at the single-cell level: an overview about state-of-the-art techniques and their limitations. *Nanomedicine* **2014**, *9*, 1885−1900.
(37) Kedmi, R.; Ben-Arie, N.; Peer, D. The systemic toxicity of positively charged lipid nanoparticles and the role of Toll-like receptor 4 in immune activation. *Biomaterials* **2010**, *31*, 6867−6875.
(38) Godbey, W. T.; Wu, K. K.; Mikos, A. G. Poly(ethylenimine)-mediated gene delivery affects endothelial cell function and viability. *Biomaterials* **2001**, *22*, 471−480.
(39) Partikel, K.; Korte, R.; Mulac, D.; Humpf, H. U.; Langer, K. Serum type and concentration both affect the protein-corona composition of PLGA nanoparticles. *Beilstein J. Nanotechnol.* **2019**, *10*, 1002−1015.
(40) Lee, S. Y.; Son, J. G.; Moon, J. H.; Joh, S.; Lee, T. G. Comparative study on formation of protein coronas under three different serum origins. *Biointerphases* **2020**, *15*, 061002.
(41) Chandran, P.; Riviere, J. E.; Monteiro-Riviere, N. A. Surface chemistry of gold nanoparticles determines the biocorona composition impacting cellular uptake, toxicity and gene expression profiles in human endothelial cells. *Nanotoxicology* **2017**, *11*, 507−519.
(42) Ha, M. K.; Kwon, S. J.; Choi, J. S.; Nguyen, N. T.; Song, J.; Lee, Y.; Kim, Y. E.; Shin, I.; Nam, J. W.; Yoon, T. H. Mass Cytometry and Single-Cell RNA-seq Profiling of the Heterogeneity in Human Peripheral Blood Mononuclear Cells Interacting with Silver Nanoparticles. *Small* **2020**, *16*, No. e1907674.
(43) Ha, M. K.; Choi, J.-S.; Kwon, S. J.; Song, J.; Lee, Y.; Kim, Y.-E.; Yoon, T. H. Mass cytometric study on the heterogeneity in cellular association and cytotoxicity of silver nanoparticles in primary human immune cells. *Environ. Sci.: Nano* **2020**, *7*, 1102−1114.
(44) Swanson, J. A. Shaping cups into phagosomes and macropinosomes. *Nat. Rev. Mol. Cell Biol.* **2008**, *9*, 639−649.
(45) Aderem, A.; Underhill, D. M. Mechanisms of phagocytosis in macrophages. *Annu. Rev. Immunol.* **1999**, *17*, 593−623.
(46) Hillaireau, H.; Couvreur, P. Nanocarriers' entry into the cell: relevance to drug delivery. *Cell. Mol. Life Sci.* **2009**, *66*, 2873−2896.

https://doi.org/10.1021/acsnanoscienceau.3c00001
ACS Nanosci. Au XXXX, XXX, XXX−XXX

(47) Lin, X. P.; Mintern, J. D.; Gleeson, P. A. Macropinocytosis in Different Cell Types: Similarities and Differences. *Membranes* **2020**, *10*, 177.
(48) Chuang, S. M.; Lee, Y. H.; Liang, R. Y.; Roam, G. D.; Zeng, Z. M.; Tu, H. F.; Wang, S. K.; Chueh, P. J. Extensive evaluations of the cytotoxic effects of gold nanoparticles. *Biochim. Biophys. Acta* **2013**, *1830*, 4960−4973.
(49) Chueh, P. J.; Liang, R. Y.; Lee, Y. H.; Zeng, Z. M.; Chuang, S. M. Differential cytotoxic effects of gold nanoparticles in different mammalian cell lines. *J. Hazard. Mater.* **2014**, *264*, 303−312.
(50) Patra, H. K.; Banerjee, S.; Chaudhuri, U.; Lahiri, P.; Dasgupta, A. K. Cell selective response to gold nanoparticles. *Nanomedicine* **2007**, *3*, 111−119.
(51) Pennock, N. D.; White, J. T.; Cross, E. W.; Cheney, E. E.; Tamburini, B. A.; Kedl, R. M. T cell responses: naive to memory and everything in between. *Adv. Physiol. Educ.* **2013**, *37*, 273−283.
(52) Berard, M.; Tough, D. F. Qualitative differences between naive and memory T cells. *Immunology* **2002**, *106*, 127−138.
(53) Holmes, N. CD45: all is not yet crystal clear. *Immunology* **2006**, *117*, 145−155.

https://doi.org/10.1021/acsnanoscienceau.3c00001
ACS Nanosci. Au XXXX, XXX, XXX−XXX